AGU PUBLICATIONS

JGR

Journal of Geophysical Research: Oceans

RESEARCH ARTICLE

10.1002/2014JC010650

ENSO and the California Current coastal upwelling response

Michael G. Jacox[1,2], Jerome Fiechter[1], Andrew M. Moore[3], and Christopher A. Edwards[3]

[1]Institute of Marine Sciences, University of California, Santa Cruz, California, USA, [2]Environmental Research Division, Southwest Fisheries Science Center, NOAA, Monterey, California, USA, [3]Ocean Sciences Department, University of California, Santa Cruz, California, USA

Key Points:
- We examine ENSO impacts on vertical transport and source water properties
- Transport-related and density-related anomalies are quantified for 1981–2010
- Circulation is from a data assimilative model and back trajectory calculations

Correspondence to:
M. G. Jacox,
mjacox@ucsc.edu

Citation:
Jacox, M. G., J. Fiechter, A. M. Moore, and C. A. Edwards (2015), ENSO and the California Current coastal upwelling response, *J. Geophys. Res. Oceans*, *120*, doi:10.1002/2014JC010650.

Received 12 DEC 2014
Accepted 28 JAN 2015
Accepted article online 5 FEB 2015

Abstract A 31 year (1980–2010) sequence of historical analyses of the California Current System (CCS) is used to describe the central CCS (35–43°N) coastal upwelling response to El Niño-Southern Oscillation (ENSO) variability. The analysis period captures 10 El Niño and 10 La Niña events, including the extreme El Niños of 1982–1983 and 1997–1998. Data-assimilative model runs and backward trajectory calculations of passive tracers are used to elucidate physical conditions and source water characteristics during the upwelling season of each year. In general, El Niño events produce anomalously weak upwelling and source waters that are unusually shallow, warm, and fresh, while La Niña conditions produce the opposite. Maximum vertical transport anomalies in the CCS occur ~1 month after El Niño peaks in midwinter, and before the onset of the upwelling season. Source density anomalies peak later than transport anomalies and persist more strongly through the spring and summer, causing the former to impact the upwelling season more directly. As nitrate concentration covaries with density in the central CCS, El Niño may exert more influence over the nitrate concentration of upwelled waters than it does over vertical transport, although both factors are expected to reduce nitrate supply during El Niño events. Interannual comparison of individual diagnostics highlights their relative impacts during different ENSO events, as well as years deviating from the canonical response to ENSO variability. The net impact of ENSO on upwelling is explored through an "Upwelling Efficacy Index", which may be a useful indicator of bottom-up control on primary productivity.

1. Introduction

The influence of the El Niño-Southern Oscillation (ENSO) on the physical and biogeochemical environment of the California Current System (CCS) is well known. Widespread impacts of the strong El Niño in 1997–1998 motivated a diverse literature addressing impacts on upwelling favorable winds [*Schwing et al*., 2002], the physical regime [*Bograd and Lynn*, 2001; *Schwing et al*., 2002], ocean chemistry [*Castro et al*., 2002; *Chavez et al*., 2002], and the biological response, from primary producers [*Kahru and Mitchell*, 2000; *Chavez et al*., 2002] to zooplankton [*Marinovic et al*., 2002; *Peterson et al*., 2002], fish [*Pearcy*, 2002], and whales [*Benson et al*., 2002].

Two primary forcing mechanisms drive changes in the California Current during El Niño: (i) thermocline depth anomalies in the tropical Pacific propagate eastward and subsequently poleward in the equatorial and coastal wave guides, and (ii) equatorward (poleward) winds decrease (increase) due to expansion of the Aleutian Low and/or contraction of the North Pacific High pressure systems. Both impacts tend to inhibit the upwelling of nutrients into the euphotic zone, and are therefore consistent with reduced primary productivity and negative impacts on higher trophic levels. However, the relative influence of each mechanism is up for debate. For example, the onset of the 1982–1983 El Niño in the CCS was alternately attributed to atmospheric [*Simpson*, 1983] and oceanic [*Huyer and Smith*, 1985] anomalies, though both effects are widely acknowledged as important [e.g., *Huyer and Smith*, 1985; *Strub and James*, 2002].

Recently, ENSO variability has been shown to correlate on multidecadal scales with upwelling favorable winds [*Macías et al*., 2012; *García-Reyes and Largier*, 2012] and vertical transport [*Jacox et al*., 2014]. However, to our knowledge, there has not been a complete description of the CCS upwelling response to El Niño and La Niña, accounting for the influences of both atmospheric and oceanic forcing over multiple events. Here,

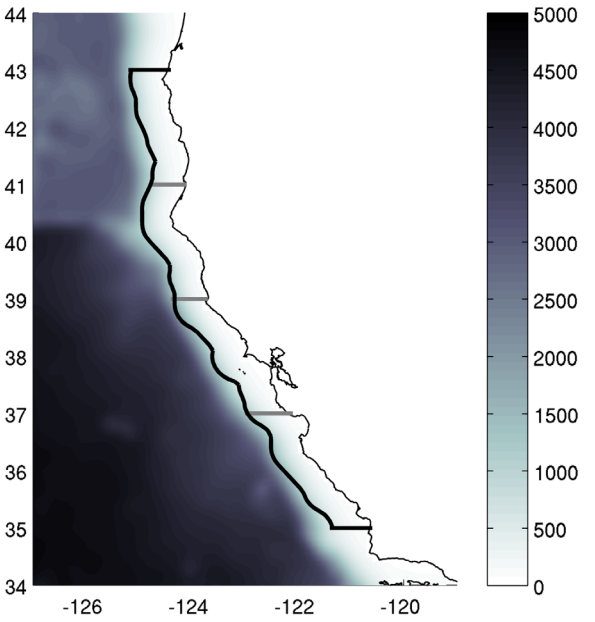

Figure 1. The central CCS portion of the model domain is shown with bottom depth (m) in color. The thick black line outlines the region of principal interest to this study, extending 35–43˚N and 0–50 km from shore. Gray lines separate the central CCS into 2˚ latitudinal subregions used for the passive tracer back trajectory calculations.

we use a data-assimilative regional ocean model, and its adjoint formulation, to determine the ENSO impacts on vertical transport, water column density, and the origins and properties of upwelled water. Passive tracers in an adjoint model have been used previously to track changes in upwelling source depth driven by the Pacific Decadal Oscillation [*Chhak and Di Lorenzo*, 2007], the North Pacific Gyre Oscillation [*Di Lorenzo et al*., 2008], and variable surface winds [*Song et al*., 2011]. Here we expand on these studies by focusing on ENSO variability while also diagnosing the density of source waters as a proxy for nutrient concentration. The diagnostics, calculated over a 30 year time period that includes 10 El Niño and 10 La Niña events, allow us to thoroughly characterize (i) the canonical upwelling response to ENSO variability in the CCS, (ii) the differences between events, and (iii) anomalous years in the historical record. While we focus on El Niño events, diagnostics are presented for all years in the record, including neutral and La Niña periods, and our findings apply across the full range of ENSO variability.

2. Methods

2.1. Numerical Model

A multidecadal (1980–2010) historical analysis of the California Current System was performed using the Regional Ocean Modeling System (ROMS) with 4D-Variational (4D-Var) data assimilation. Interannual physical variability in the coastal regime is reliably reproduced by the model [*Schroeder et al*., 2014], which has also been used previously to describe upwelling in the CCS as it relates to decadal climate variability [*Jacox et al*., 2014]. Since the full model configuration and assimilation system are described in detail elsewhere [*Moore et al*., 2013], we provide only a brief summary here.

The model domain spans the west coast of the United States from 30 to 48˚N and 115 to 134˚W at 0.1˚ horizontal resolution with 42 terrain-following levels in the vertical. The present study is focused on the central CCS subregion of the domain, depicted in Figure 1. Surface winds are taken from the European Centre for Medium-range Weather Forecasting (ECMWF) 40 year reanalysis (ERA 40) for 1980–1987 and from the Cross-Calibrated Multiplatform (CCMP) [*Atlas et al*., 2011] wind product for 1988–2010. Heat, freshwater, and radiative surface fluxes are provided by ERA 40 [*Uppala et al*., 2005] for 1980–2001 and ERA Interim [*Dee et al*., 2011] for 2002–2010.

The dual formulation of 4D-Var is used to correct model initial conditions, boundary conditions, and surface forcing in overlapping 8 day analysis cycles. Assimilated data products include satellite SST (Advanced Very High Resolution Radiometer (AVHRR) Pathfinder, Advanced Microwave Scanning Radiometer-EOS (AMSR-E), and Moderate Resolution Imaging Spectroradiometer (MODIS) Terra), satellite SSH (Archiving, Validation, and Interpretation of Satellite Oceanographic data (AVISO)), and in situ temperature and salinity (expendable bathythermographs, mechanical bathythermographs, conductivity-temperature-depth sensors, and Argo profiling floats) from version 2a of the quality-controlled ENSEMBLES (EN3) data set [*Ingleby and Huddleston*, 2007].

2.2. Back Trajectories of Passive Tracers

Source waters for central CCS upwelling are characterized using the adjoint of the ROMS tangent linear model [*Moore et al*., 2004]. Adjoint methods have been employed in a number of ocean model sensitivity

studies, including application to several aspects of the CCS circulation [*Moore et al*., 2009; *Veneziani et al*., 2009]. In such studies, the adjoint quantifies the sensitivity of a circulation metric to perturbations in the model initial condition, boundary conditions, and external forcing. In the present study and several others [*Chhak and Di Lorenzo*, 2007; *Song et al*., 2011], the ROMS adjoint is used in a different capacity, which is to compute back trajectories of passive tracers. In this configuration, passive tracers are propagated backward in time from a specified region, thereby tracking the water masses in that region back to their origin at an earlier time. Back trajectories have been widely used in atmospheric science [*Stohl*, 1998], and back trajectories based on the ROMS adjoint formulation have been used to elucidate the origins of upwelled waters and how they change in response to decadal-scale climate fluctuations [*Chhak and Di Lorenzo*, 2007], surface forcing [*Song et al*., 2011], and ENSO variability (this study). Details of the configuration for passive tracer back trajectory calculations in ROMS are provided in *Song et al*. [2011], and the calculations reported here ensure conservation of the passive tracer through time. The 4D-Var analyses described in section 2.1 provide the ocean circulation fields needed for the back trajectory runs. For each month of the 30 year analysis, an initial condition for the back trajectory is created by seeding a passive tracer in the upwelling zone (Figure 1) for one 8 day assimilation cycle. Each run is then integrated backward in time for 1 month, enabling characterization of source waters 1 month prior to their appearance nearshore in the surface mixed layer.

As in *Chhak and Di Lorenzo* [2007] and *Song et al*. [2011], we consider the distribution of passive tracers at a specified time prior to arrival in the surface mixed layer of specific coastal regions. However, we also quantify the properties of water masses associated with those sources, as detailed in section 2.3. The region of particular interest to this study is the central CCS from Point Conception to Cape Blanco (35–43°N), a region where *Jacox et al*. [2014] found coherent spatial patterns and interannual variability in coastal upwelling, and which we find to also behave in a qualitatively coherent manner in terms of upwelling source water properties. For the passive tracer back trajectory calculations, we further divide the central CCS region into 2° latitude bins (Figure 1) to quantify changes in the local magnitude and timing of El Niño effects along the coast.

2.3. Upwelling Metrics

The results presented herein focus on a suite of circulation metrics chosen to characterize the upwelling response. Diagnostics calculated directly from the ocean state are intended to capture effects of the atmospheric anomaly associated with El Niño and the oceanic anomaly that propagates from the tropics. Though the upwelling circulation and density structure are each influenced by both the oceanic and atmospheric teleconnections, we assume that wind-driven vertical transport, W, is associated primarily with atmospheric anomalies while the depth of the 26.0 kg m^{-3} potential density surface, $d_{26.0}$ (approximating the depth of the pycnocline), is driven primarily by remote oceanic forcing. This assumption is supported by the lags observed in W and $d_{26.0}$ relative to tropical Pacific SST anomalies, as described in section 3.1. The passive tracer back trajectory calculations are used to characterize upwelling source waters, specifically their depth, d_s, and potential density, σ_s. Each calculation is integrated backward in time for 1 month, such that source water diagnostics represent the mean properties of upwelled water 1 month prior to arrival in the target region (Figure 1). For example, the mean source density σ_s at time t is calculated from the tracer field at time (t – 1 month) as follows:

$$\sigma_s = \frac{\sum_{i=1}^{N} (T_i \cdot V_i \cdot \sigma_i)}{\sum_{i=1}^{N} (T_i \cdot V_i)}$$

where T_i is the tracer concentration in cell i, V_i is cell volume, σ_i is the cell density, and summations are performed over all N grid cells in the model domain. Source depth is calculated similarly, with σ replaced by d.

A back trajectory calculation started at the beginning of a given month provides a solution for the start of the previous month, and the metrics W and $d_{26.0}$ are averaged monthly. In this manner, the tracer source properties are aligned with the mean physical environment during the 1 month back trajectory integration period. For example, a back trajectory starting at the beginning of June is analyzed at the beginning of May, and is considered relative to the mean physical environment in May.

The results in section 3.1 are concerned primarily with monthly data in 2° alongshore subregions extending 50 km offshore (Figure 1), for which anomalies are computed by removing the mean seasonal cycle. In

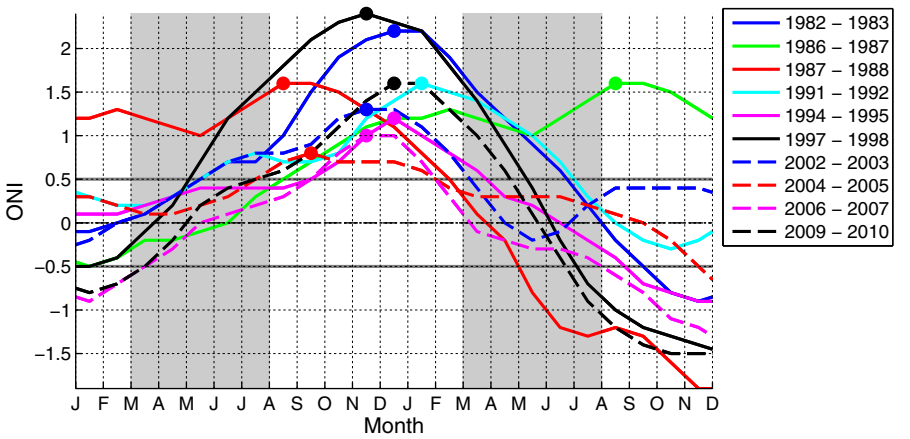

Figure 2. Two-year progression of the Oceanic Niño Index (ONI) for each El Niño event in the analysis period. Colored dots mark the peak ONI value for each El Niño event. Horizontal gray lines indicate thresholds the ONI must remain above (below) for five consecutive months in order to qualify as El Niño (La Niña) events. The central CCS upwelling season is shaded in gray.

section 3.2, we consider the entire central CCS (35–43°N) coastal band as a single region and focus on interannual upwelling variability. To that end, for section 3.2, the monthly metrics are averaged over the upwelling season, which runs from March to July as defined by peak vertical transports in the analysis region. For both monthly and interannual analyses, time series are detrended to isolate the relatively high-frequency El Niño signal from longer-term upwelling variability and trends.

The Upwelling Efficacy Index (UEI) described in section 3.3 is defined as the first principal component of the four key upwelling metrics described here (W, $d_{26.0}$, d_s, σ_s), each of which was first standardized by removing its mean and dividing by its standard deviation. Chlorophyll data used for comparison with the UEI is the Sea-viewing Wide Field-of-view Sensor (SeaWiFS) level 2 global monthly composite chlorophyll-a, downloaded from NOAA CoastWatch.

2.4. El Niño Events

We define El Niño events based on the Oceanic Niño Index (ONI) produced by NOAA, which is defined as the 3 month running mean of SST anomaly in the NINO3.4 region. An El Niño event occurs when the ONI reaches 0.5°C for a minimum of five consecutive months. Ten El Niño events are captured by our analysis period, and the progression of each is illustrated in Figure 2. El Niño events typically reach their peak magnitude in winter, with a return to neutral ONI values by early summer. However, some El Niños may end as early as February and may additionally be followed immediately by La Niña conditions. While these events qualify as El Niños based on tropical Pacific SST anomalies, they have very different implications for upwelling in the central CCS, which is strongest from March to July. Therefore, when defining El Niño events for our analysis, we apply the usual criteria of ONI $\geq$ 0.5°C for at least five consecutive months, with the additional stipulation that the mean ONI during the central CCS upwelling season (March–July) be greater than zero. Thus, our analysis excludes the 1987–1988 and 2006–2007 El Niños, which ended unusually early in the year and were immediately followed by cold SST anomalies in the tropics. Similarly for La Niña, requiring the mean ONI to be less than zero during the upwelling season excludes the 2008–2009 event.

3. Results

3.1. El Niño Timing and the Local Upwelling Response

Figure 3 summarizes the climatological upwelling signature in the central CCS as well as anomalies introduced by El Niño events. In general, El Niño generates a deep pycnocline and weak upwelling (or downwelling), and surface waters carry the signature of a relatively rare and shallow source (note that here the word rare is used in its original meaning as the opposite of dense, or more specifically "having the constituent material or particles loose or not closely packed together; not dense or compact; attenuated" [*OED online*, 2014]). These effects first appear in winter, coincident with maximum tropical SST anomalies as indicated by the ONI (Figure 2).

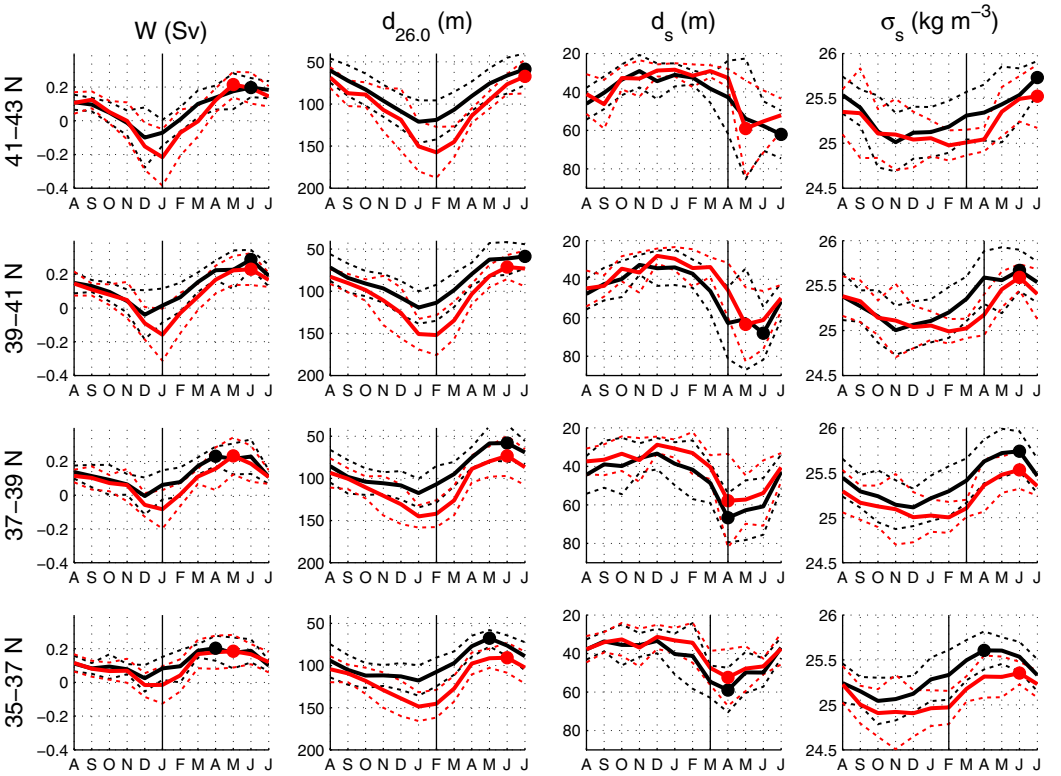

Figure 3. Monthly climatology of vertical transport (W), pycnocline depth ($d_{26.0}$), source depth (d_s), and source density (σ_s) for neutral ONI years (black) and for El Niño years (red) in each 2° latitude bin from 35–43°N. Dotted lines indicate ± one standard deviation of the values for each month. Colored dots mark upwelling season minima or maxima of each time series. Vertical black lines indicate months of greatest difference between El Niño and neutral years. Note the time axis runs August–July to reflect the typical timing of El Niño events and their impact on coastal upwelling.

At all latitudes, January is the least favorable month for upwelling; the south of the domain sees its weakest upwelling of the year, while the north of the domain sees its strongest downwelling (Figure 3, black lines). Conversely, the timing of the peak upwelling season is latitude-dependent, shifting from March/April off central California to June/July off southern Oregon. Source depth closely tracks vertical transport, with a marked increase after the spring transition that denotes the onset of seasonal upwelling. However, it should be noted that the mean source depth is representative of all source waters, not just those that have been upwelled. The source depth of upwelled waters is therefore greater than the source depth reported here. Source depths during winter (∼ 30 m) indicate shallow origins, with nearshore water deriving largely through lateral advection from adjacent regions (Figure 4). Deeper source depths in spring and summer indicate a greater contribution from upwelling. Peak source depths are reached earlier in the southern part of the study region, consistent with the latitudinal progression of the timing of the upwelling season. Pycnocline depth evolves similarly on seasonal timescales, deepest in midwinter and shallowest in late spring to early summer, although it is not as closely tied to vertical transport as is source depth. The source density of upwelled water depends on both the magnitude of vertical transport and the water column density profile, and it therefore reflects variability in both. Consequently, peak source density occurs later in the year at more northern latitudes, coincident with the local timing of strongest upwelling.

While the timing of seasonal upwelling clearly depends on latitude, the same dependence is not seen in vertical transport anomalies (Figure 3). Peak tropical SST anomalies in November/December (Figure 2) are followed by the largest central CCS vertical transport anomalies in January. As vertical transport variability in the study region is strongly correlated to local wind forcing [*Jacox et al.*, 2014], the timing of vertical transport anomalies likely indicates a rapid atmospheric teleconnection from the tropics to the U. S. west coast. The atmospheric bridge responds to tropical anomalies in as little as 2 weeks [*Alexander et al.*, 2002], and we see maximum correlation of the ONI with vertical transport anomalies at 1–2 months lag (Table 1). As a result, the greatest El Niño-related anomalies in vertical transport do not impact the upwelling season

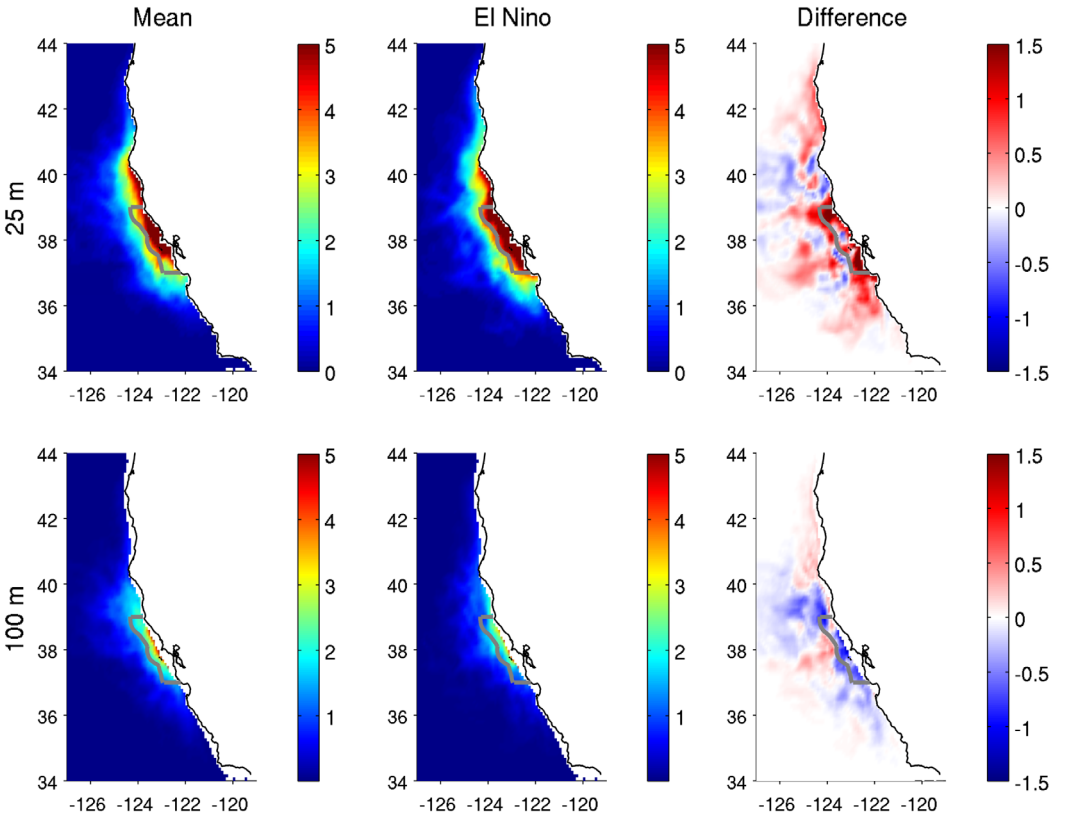

Figure 4. Mean tracer distribution 1 month prior to arrival in the upper 20 m of the region indicated by gray outline. Tracer concentration is shown at (top) 25 m and (bottom) 100 m depth, and is averaged over March–July of (left) neutral ONI years and (middle) El Niño years. (right) Positive (negative) values indicate higher (lower) than average concentration during El Niño, i.e., more (less) water originating from this location. As the total amount of tracer in the domain is arbitrary, concentrations are informative in a comparative (not absolute) sense.

directly. In fact, the most noticeable effect of El Niño is to produce strong wintertime downwelling in the northern regions, and little to no net vertical transport in the southern part of the domain. While the spring/summer months are also characterized by anomalously weak coastal upwelling, consistent with previous studies [*Schwing et al.*, 2002; *García-Reyes and Largier*, 2012; *Jacox et al.*, 2014], the impact is of lower magnitude than the wintertime effect. As a result, El Niño may impact coastal upwelling more strongly at the southern end of the CCS, where the onset of the upwelling season occurs closer to the time of greatest El Niño-related anomalies.

Table 1. Lagged Correlations of Upwelling Anomalies With the ONI[a]

	Monthly Mean		Upwelling Season Mean	
	r	Lag (months)	r	Lag (months)
W (Sv)	−0.26	1–2	**−0.55**	1
$d_{26.0}$ (m)	**0.54**	2–3	**0.60**	2
d_s (m)	−0.23	2	**−0.52**	1–2
σ_s (kg m^{-3})	**−0.42**	3–4	**−0.60**	2–4

[a]Correlation coefficient (r) and lag between the ONI and four metrics of upwelling dynamics described in section 2.3: vertical transport across the 40 m depth level (W), depth of the 26.0 kg m^{-3} potential density surface ($d_{26.0}$), mean source depth (d_s), and mean source density (σ_s). Correlations and lags are shown for monthly data as well as for annual upwelling season (March–July) means. In both cases, variables are averaged over our full central CCS coastal domain (35–43°N, 0–50 km from shore). When multiple lags produce the same correlation (to two significant digits), all are listed. Bold correlations are significant above the 95% level.

Pycnocline depth anomalies propagate poleward via the coastal wave guide at speeds of 35–180 km day^{-1} [*Enfield and Allen*, 1980; *Chelton and Davis*, 1982], implying time scales of one to 6 months for travel to the central CCS. We find maximum correlation of the ONI with pycnocline depth anomalies at 2–3 months lag (Table 1), and pycnocline depth anomalies peak in February, 1 month later than transport anomalies (Figure 3). Similarly, source density anomalies peak in late winter/early spring and remain through summer. These oceanic anomalies are more persistent through spring and summer than vertical transport anomalies associated with atmospheric

Table 2. Upwelling Anomalies Associated With El Niño and La Niña Events[a]

	Mean	EN Anomaly	EN Anomaly Ratio	LN Anomaly	LN Anomaly Ratio
SST (°C)	12.2	**+0.6**	1.1	−0.3	0.5
W (Sv)	0.71	**−0.14**	1.0	+0.10	0.7
$d_{26.0}$ (m)	76.9	**+19.7**	1.8	−1.9	0.2
d_s (m)	52.4	**−6.2**	1.0	+2.9	0.5
σ_s (kg m^{-3})	25.51	**−0.22**	1.4	+0.06	0.4
Deep water (%)	58.3	**−6.0**	0.9	+1.9	0.3

[a]Upwelling season (March–July) mean conditions for neutral ONI periods, as well as El Niño (EN) and La Niña (LN) anomalies relative to neutral conditions. Data are shown for the variables described in Table 1, as well as sea surface temperature (SST) and the percentage of coastal surface water originating from greater than 40 m depth (deep water). All values are averaged over the region 35–43°N and 0–50 km from shore. Anomaly ratios are defined as El Niño/La Niña anomalies divided by the standard deviation of values during neutral ONI periods. They provide a relative measure of anomaly magnitudes. For example, the El Niño SST anomaly ratio of 1.1 indicates that during El Niño years the sea surface is on average 1.1 standard deviations warmer than it is during neutral ONI conditions. Anomalies that are statistically different from neutral conditions at the 95% significance level (determined by a two-sample t-test) are indicated in bold.

forcing. The discrepancy is likely tied to variability in the North Pacific High, whose contraction during El Niño drives the weakening of equatorward winds [*Simpson*, 1983]. The North Pacific High is the dominant control on alongshore wind variability in the winter [*García-Reyes et al*., 2013], and its interannual variance is much higher during winter (January–March) than during spring/summer (April–July), consistent with the seasonal magnitude of transport anomalies (Figure 3). While El Niño impacts coastal upwelling through anomalies in both oceanic and atmospheric forcing, the oceanic influence may be greater due to these differences in timing (Table 2).

3.2. Interannual Variability

Figure 4 shows the mean of passive tracer distribution for a representative portion of the central CCS coast during neutral ONI years, as well as the typical El Niño distribution. During El Niño events, a lower fraction of the nearshore surface mixed layer derives from deep water masses (Figure 4 and Table 2). The influence of lateral advection relative to upwelling is increased, with anomalously high tracer concentrations originating in near-surface waters to the north and, to a lesser degree, offshore and to the south. Though we previously showed regional differences in the timing of upwelling relative to the El Niño influence, the qualitative response described here is consistent throughout the central CCS and interannual variability is coherent over the broader region outlined in Figure 1. For the remainder of the analysis, we therefore consider the entire central CCS as one region and examine diagnostic variables averaged over the peak upwelling season, which is defined here as March–July.

Mean upwelling season source depths during individual El Niño events (as well as neutral and La Niña periods) are presented in Figure 5. There is considerable scatter, with peak-to-peak changes of ~20 m between years (for reference, typical mean source depths during the upwelling season are 50–60 m, Figure 3). The influence of El Niño on source depth is unmistakable, as five of the six most anomalously shallow years are El Niños. Similarly, the regimes of especially weak transport, deep pycnoclines, and rare source waters are dominated by El Niño years. These relationships are further supported by direct correlations of the ONI with upwelling-related anomalies, which are all significant at $r \approx 0.6$ (Figure 6). Figure 6 also shows the consistency of the upwelling-ONI relationship across all years, not just El Niño years. Periods of anomalously cold SST in the tropical Pacific (negative ONI, La Niña conditions) tend to produce the opposite anomalies from El Niño—strong upwelling, a shallow pycnocline, and deep, dense source waters, though the impact is not as great as it is during El Niño (Figure 5 and Table 2).

While the response to any given El Niño event is likely to be qualitatively the same, the relative impact on different aspects of the upwelling circulation is variable. For example, the 2002–2003 event resulted in weak upwelling during the 2003 upwelling season, but no visible deviation from the mean pycnocline depth. In contrast, the strong 1982–1983 event generated an exceptionally deep pycnocline with only slightly weaker than average upwelling, consistent with the assertion of *Huyer and Smith* [1985] that remotely forced ocean anomalies triggered that event in the CCS. Part of the discrepancy between vertical transport and pycnocline depth relates to low-frequency variability. The five events occurring from 1992 to

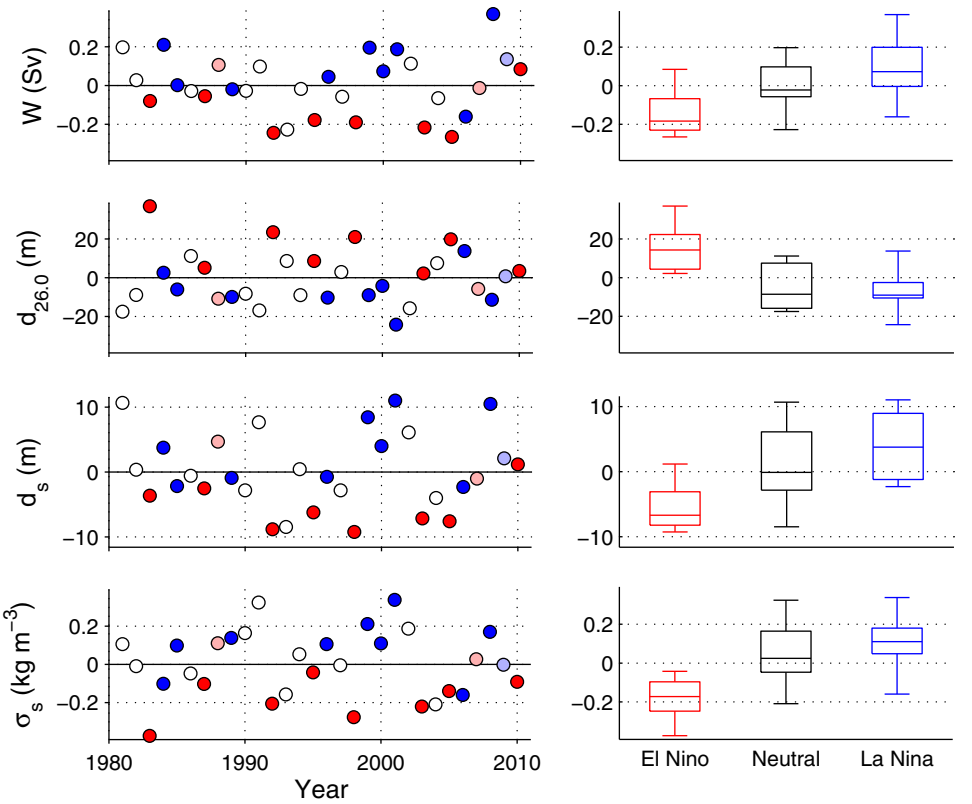

Figure 5. (left) Detrended upwelling season anomalies of vertical transport (W), pycnocline depth ($d_{26.0}$), source depth (d_s), and source density (σ_s). Red dots are El Niño years, blue dots are La Niña years, and pale red (blue) dots are El Niño (La Niña) years that do not meet our additional criteria of ONI>0 (ONI<0) for the upwelling season. (right) Boxplots indicating range and quartiles of each variable for El Niño, La Niña, and neutral years.

2005 generated large transport anomalies, while the pre-1992 and post-2005 events produced little effect. No such low-frequency signal is visible in pycnocline depth and source density.

A number of years defy the canonical upwelling response to El Niño: either El Niño years that do not induce the characteristic El Niño anomalies (1988, 2007, 2010), or neutral years that are El Niño-like in terms of upwelling anomalies (1993, 2004, 2006). However, much of this apparent discrepancy disappears if ONI values are considered specifically for the upwelling season. As discussed previously, both the 1987–1988 and 2006–2007 El Niños ended early in the year and were followed immediately by cold SST anomalies, such that conditions during the upwelling season were not indicative of El Niño (Figure 6). Similarly, the 1992–1993 season very nearly met the ONI definition of El Niño, with four consecutive months of ONI $\geq$ 0.5. In Figure 6, it is the non-El Nino year with highest ONI values, and based on the upwelling season is more El Niño-like than a number of the ONI-defined El Niño years. The 2003–2004 season also saw warm tropical SST anomalies, though not to the same degree. Two years, 2006 and 2010, are not easily reconciled with the ONI. In these cases, the model results indicate that the dominant drivers of local upwelling circulation and hydrography are not associated with ENSO.

3.3. An Upwelling Efficacy Index

To explore the joint impact of vertical transport and source water composition, we construct an "Upwelling Efficacy Index" (UEI, Figure 7), defined as the first principal component of our four explanatory variables (W, $d_{26.0}$, d_s, and σ_s), each standardized (zero mean, unit variance) before computing the UEI. The UEI captures 84% of the variance in its four constituent variables and correlates with each of them at r $\geq$ 0.9. Inasmuch as density is a proxy for nitrate supply, the UEI is a proxy for nitrate flux during upwelling, which depends on both vertical transport and nitrate concentration in source waters. Negative values of the UEI indicate anomalously low nitrate flux into the mixed layer from below. Such years are dominated by El Niño events, consistent with the findings of Figure 5. Interestingly, the three most impactful El Niño events (1982–1983,

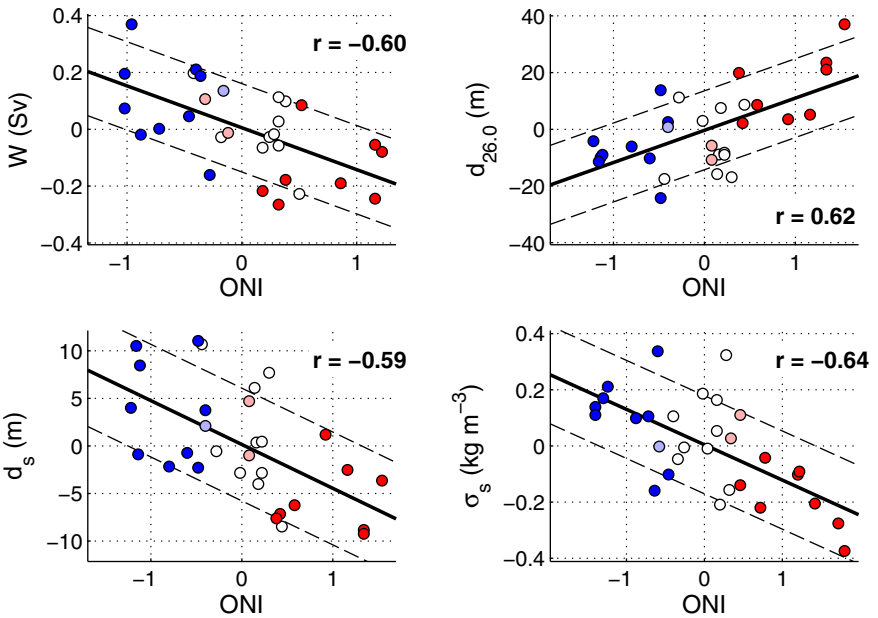

Figure 6. Upwelling season (March–July) anomalies of vertical transport (W), pycnocline depth ($d_{26.0}$), source depth, and source density plotted against the ONI. W correlates most strongly with the ONI at one month lag, $d_{26.0}$ and d_s lag the ONI by two months, and σ_s has a 3 month lag. Therefore, the ONI averaging period is February–June for W, January–May for $d_{26.0}$ and d_s, and December–April for σ_s. Dashed lines indicate ± one standard deviation of the dependent variable. Dots are colored as in Figure 5.

1991–1992, 1997–1998) are identified by the UEI as having nearly identical influence over upwelling efficacy, though the mechanisms are quite different. The pycnocline depth and resultant source density anomaly were exceptional in 1983, while vertical transport was only slightly below average. In 1992 and 1998, both density and transport anomalies contributed substantially to the low UEI, with a slightly larger transport effect in 1992 and a slightly larger density effect in 1998. The biological impact of different El Niño events could therefore be similar even though the related forcing mechanisms (oceanic versus atmospheric) may be different. On interannual timescales, the UEI is significantly correlated (r = 0.72) with chlorophyll biomass (Figure 7), suggesting bottom-up control of primary productivity in this region.

4. Discussion

We have presented a description of the canonical coastal upwelling response to ENSO variability in the central CCS, as well as signatures associated with specific events. Output from a data-assimilative regional

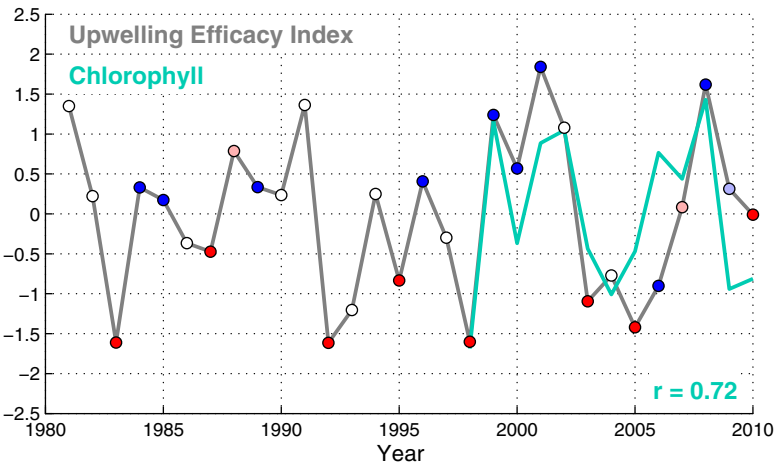

Figure 7. Time series of the Upwelling Efficacy Index (gray) and SeaWiFS chlorophyll (green). Chlorophyll is averaged from March to July, and over the region 35–43°N and 0–300 km from shore. Dots are colored as in Figure 5.

ocean model was used to characterize the upwelling circulation and hydrography, while the properties of upwelling source waters were diagnosed by back trajectory calculations. In general, coastal upwelling is weaker during El Niño, the pycnocline deepens, and source waters are rarer and shallower. The magnitude of anomalies is related to El Niño strength and anomalies of the opposite sign are associated with La Niña events (Figures 5 and 6, Table 2). Importantly, the assimilation of available data allows us to better constrain anomalies that originate outside of the model domain and are not fully resolved through the boundary conditions at 0.1° resolution. El Niño-related anomalies in forward model runs are of lower magnitude than those in the analyses (not shown), indicating that information missing from the oceanic teleconnection in forward runs is being imparted by data assimilation.

The two source water properties highlighted here, depth and density, are each linked differently to environmental conditions. Specifically, source depth anomalies are more strongly correlated to W ($r = 0.93$) than to $d_{26.0}$ ($r = -0.75$), while source density anomalies are more strongly correlated to $d_{26.0}$ ($r = -0.90$) than to W ($r = 0.68$). This result is attributed to the different timescales of atmospheric teleconnections (which drive transport anomalies through expansion of the Aleutian Low and contraction of the North Pacific High pressure systems) and remote oceanic forcing (which drives density anomalies through equatorial and coastal wave-guide propagation). The atmosphere responds to tropical SST anomalies in approximately 2 weeks [*Alexander et al*., 2002] while oceanic propagation occurs on the order of months [*Enfield and Allen*, 1980; *Chelton and Davis*, 1982]. Furthermore, during El Niño substantially more high-frequency variability is present in the wind than in SST [*Schwing et al*., 2002, Figure 5]. Since tropical SST anomalies peak in winter, and oceanic anomalies in the CCS have a later onset and greater persistence than atmospheric anomalies, the spring/summer upwelling season may be more directly impacted through oceanic forcing than wind forcing (Table 2). Similarly, since the onset of upwelling is earlier in the southern portion of the CCS, it may be more susceptible to El Niño impacts, which are most significant in the late winter and early spring.

Reductions in vertical transport and source density during El Niño are both expected to decrease nitrate supply and, consequently, biological production. An in-depth analysis of nitrate flux using robust nitrate models [e.g., *Palacios et al*., 2013] is left to a later study; however, we speculate here based on the assumption that density is a good proxy for nitrate concentration. Total nitrate flux due to upwelling is the product of vertical transport and nitrate concentration in upwelled waters. Therefore, years in which both transport and source density are low should have the lowest nitrate supply, and vice versa for years with strong upwelling and dense source waters. Similarly, different years could produce equal nitrate flux even though they have different vertical transports and source densities. For example, the source density in 1983 suggests very low nitrate concentration in source waters, while upwelling strength was near the long-term mean. In 1998, our results suggest that source waters were likely more nitrate-rich than in 1983, while upwelling was weaker. Nitrate flux, and consequently potential new production, may be approximately equal under these two scenarios. Correlation of the UEI with chlorophyll biomass in the central CCS supports this hypothesis of bottom-up control on productivity (Figure 7). However, there is evidence for regulation of new production by factors beyond nutrient supply [e.g., *Messié and Chavez*, 2014], and individual components of the UEI may affect biology in disparate ways. For example, strong upwelling conditions and associated turbulence can suppress primary productivity through light limitation [*Huntsman and Barber*, 1977]. While correlation of the UEI with chlorophyll biomass is intriguing, exploration of individual and joint drivers of primary production in the CCS is ongoing.

Several studies on decadal-scale climate variability and its impacts on upwelling have found responses similar to those we see related to ENSO [e.g. *Chhak and Di Lorenzo*, 2007; *Di Lorenzo et al*., 2008; *Macías et al*., 2012; *Jacox et al*., 2014]. In particular, the Pacific Decadal Oscillation (PDO) and ENSO correlate with upwelling variables in qualitatively the same way. The relative influence of each is therefore difficult to discern, and they are not independent; the strongest eastern Pacific El Niños are more likely to occur during positive phases of the PDO [*Verdon and Franks*, 2006]. While correlation of the ONI and PDO during our analysis period is only moderately strong ($r = 0.53$), the PDO is positive during the upwelling season of all 10 El Niño events; this relationship further obscures the influence of each. However, the seasonal progression of upwelling-related anomalies (Figure 3) and their lags relative to tropical Pacific anomalies (Table 1) are both consistent with ENSO forcing. Interestingly, the UEI is equally well correlated ($r = 0.67$) to the ONI (at 2 month lag) and the PDO (at zero lag), suggesting that it captures upwelling variability associated with both climate indices independently of each other.

Finally, the analysis presented here is focused on the spring/summer upwelling season, when large nutrient pulses from below the surface mixed layer stimulate growth of primary producers that form the base of the marine food chain. However, several studies implicate winter conditions, particularly upwelling, in the reproductive timing and success of marine predators including several species of rockfish and seabirds [*Schroeder et al*., 2009; *Black et al*., 2011]. Given that the impacts of El Niño on upwelling (and downwelling) during winter are qualitatively similar and generally more pronounced than during the spring/summer upwelling season (Figure 3), the dynamics described herein are likely to impact a wide range of species over multiple trophic levels, each of which may respond to upwelling through distinct mechanisms.

Acknowledgments
The model output used for analysis herein is available from http://oceanmodeling.ucsc.edu. We are grateful for the support of the National Science Foundation (OCE 1061434). We also thank two reviewers for comments that helped improve the manuscript.

References

Alexander, M. A., I. Bladé, M. Newman, J. R. Lanzante, N.-C. Lau, and J. D. Scott (2002), The atmospheric bridge: The influence of ENSO teleconnections on air-sea interaction over the global oceans, *J. Clim.*, *15*, 2205–2231.

Atlas, R., R. N. Hoffman, J. Ardizzone, S. M. Leidner, J. C. Jusem, D. K. Smith, and D. Gombos (2011), A cross-calibrated, multiplatform ocean surface wind velocity product for meteorological and oceanographic applications, *Bull. Am. Meteorol. Soc.*, *92*, 157–174, doi:10.1175/2010BAMS2946.1.

Benson, S. R., D. A. Croll, B. B. Marinovic, F. P. Chavez, and J. T. Harvey (2002), Changes in the cetacean assemblage of a coastal upwelling ecosystem during El Niño 1997–98 and La Niña 1999, *Prog. Oceanogr.*, *54*, 279–291.

Black B. A., I. D. Schroeder, W. J. Sydeman, S. J. Bograd, B. K. Wells, and F. B. Schwing (2011), Winter and summer upwelling modes and their biological importance in the California Current Ecosystem, *Global Change Biol.*, *17*, 2536–2545.

Bograd, S. J., and R. J. Lynn (2001), Physical-biological coupling in the California Current during the 1997–99 El Niño-La Niña cycle, *Geophys. Res. Lett.*, *28*, 275–278, doi:10.1029/2000GL012047.

Castro, C. G., C. A. Collins, P. Walz, J. T. Pennington, R. P. Michisaki, G. Friederich, and F. P. Chavez (2002), Nutrient variability during El Niño 1997–1998 in the California current system off central California, *Prog. Oceanogr.*, *54*, 171–184.

Chavez, F. P., J. T. Pennington, C. G. Castro, J. P. Ryan, R. P. Michisaki, B. Schlining, P. Walz, K. R. Buck, A. McFadyen, and C. A. Collins (2002), Biological and chemical consequences of the 1997–1998 El Niño in central California waters, *Prog. Oceanogr.*, *54*, 205–232.

Chelton, D. B., and R. E. Davis (1982), Monthly mean sea-level variability along the west coast of North America, *J. Phys. Oceanogr.*, *12*, 757–784.

Chhak, K., and E. Di Lorenzo (2007), Decadal variations in the California Current upwelling cells, *Geophys. Res. Lett.*, *34*, L14604, doi:10.1029/2007GL030203.

Dee, D. P., et al. (2011), The ERA-Interim reanalysis: Configuration and performance of the data assimilation system, *Q. J. R. Meteorol. Soc.*, *137*, 553–597.

Di Lorenzo, E., et al. (2008), North Pacific Gyre oscillation links ocean climate and ecosystem change, *Geophys. Res. Lett.*, *35*, L08607, doi:10.1029/2007GL032838.

Enfield, D. B., and J. S. Allen (1980), On the structure and dynamics of montly mean sea level anomalies along the Pacific coast of North and South America, *J. Phys. Oceanogr.*, *10*, 557–578.

García-Reyes, M., and J. Largier (2012), Seasonality of coastal upwelling off central and northern California: New insights, including temporal and spatial variability, *J. Geophys. Res.*, *117*, C03028, doi:10.1029/2011JC007629.

García-Reyes, M., W. J. Sydeman, B. A. Black, R. R. Rykaczewski, D. S. Schoeman, S. A. Thompson, and S. J. Bograd (2013), Relative influence of oceanic and terrestrial pressure systems in driving upwelling-favorable winds, *Geophys. Res. Lett.*, *40*, 5311–5315, doi:10.1002/2013GL057729.

Huntsman, S. A., and R. T. Barber (1977), Primary production off northwest Africa: The relationship to wind and nutrient conditions. *Deep Sea Res.*, *24*, 25–33.

Huyer, A., and R. L. Smith (1985). The signature of El Nino off Oregon in 1982–83, *J. Geophys. Res.*, *90*, 7133–7142.

Ingleby, B., and M. Huddleston (2007), Quality control of ocean temperature and salinity profiles: Historical and real-time data, *J. Mar. Syst.*, *65*, 158–175.

Jacox, M. G., A. M. Moore, C. A. Edwards, and J. Fiechter (2014), Spatially resolved upwelling in the California Current System and its connections to climate variability, *Geophys. Res. Lett.*, *41*, 3189–3196, doi:10.1002/2014GL059589.

Kahru, M., and B. G. Mitchell (2000), Influence of the 1997–98 El Nino on the surface chlorophyll in the California Current, *Geophys. Res. Lett. 27*, 2937–2940, doi:10.1029/2000GL011486.

Macías, D., M. R. Landry, A. Gershunov, A. J. Miller, and P. J. S. Franks (2012), Climatic control of upwelling variability along the western North-American coast, *PLoS One*, *7*, e30436, doi:10.1371/journal.pone.0030436.

Marinovic, B. B., D. A. Croll, N. Gong, S. R. Benson, and F. P. Chavez (2002), Effects of the 1997–1999 El Niño and La Niña events on zooplankton abundance and euphausiid community composition within the Monterey Bay coastal upwelling system, *Prog. Oceanogr.*, *54*, 265–277.

Messié, M., and F. P. Chavez (2014), Seasonal regulation of primary productivity in eastern boundary upwelling systems, *Prog. Oceanogr.*, doi:10.1016/j.pocean.2014.10.011.

Moore, A. M., H. G. Arango, E. Di Lorenzo, B. D. Cornuelle, A. J. Miller, and D. J. Neilson (2004), A comprehensive ocean prediction and analysis system based on the tangent linear and adjoint of a regional ocean model, *Ocean Modell.*, *7*, 227–258.

Moore, A. M., H. G. Arango, E. Di Lorenzo, A. J. Miller, and B. D. Cornuelle (2009), An adjoint sensitivity analysis of the southern California Current circulation and ecosystem, *J. Phys. Oceanogr.*, *39*, doi:10.1175/2008JPO3740.1

Moore, A. M., C. Edwards, J. Fiechter, P. Drake, H. G. Arango, E. Neveu, S. Gürol, and A. T. Weaver (2013), A 4D-Var analysis system for the California Current: A prototype for an operational regional ocean data assimilation system, in *Data Assimilation for Atmospheric, Oceanic and Hydrologic Applications*, vol. 2, edited by S. K. Park and L. Xu, pp. 345–366, Springer, Berlin.

OED online (2014), s.v., ''rare''. [Available at http://www.oed.com/view/Entry/158248, last accessed 20 Nov. 2014.]

Palacios, D. M., E. L. Hazen, I. D. Schroeder, and S. J. Bograd (2013), Modeling the temperature-nitrate relationship in the coastal upwelling domain of the California Current, *J. Geophys. Res. Oceans*, *118*, 3223–3239, doi:10.1002/jgrc.20216.

Pearcy, W. G. (2002), Marine nekton off Oregon and the 1997–98 El Nino, *Prog. Oceanogr.*, *54*, 399–403.

Peterson, W. T., J. E. Keister, and L. R. Feinberg (2002), The effects of the 1997–99 El Niño/La Niña events on hydrography and zooplankton off the central Oregon coast, *Prog. Oceanogr. 54*, 381–398.

Schroeder, I. D., W. J. Sydeman, N. Sarkar, S. A. Thompson, S. J. Bograd, and F. B. Schwing (2009), Winter pre-conditioning of seabird phenology in the California Current, *Mar. Ecol. Prog. Ser.*, *393*, 211–223.

Schroeder, I. D., J. A. Santora, A. M. Moore, C. A. Edwards, J. Fiechter, E. L. Hazen, S. J. Bograd, J. C. Field, and B. K. Wells (2014), Application of a data-assimilative regional ocean modeling system for assessing California Current System ocean conditions, krill, and juvenile rockfish interannual variability, *Geophys. Res. Lett.*, *41*, 5942–5950, doi:10.1002/2014GL061045.

Schwing, F. B., T. Murphree, L. deWitt, and P. M. Green (2002), The evolution of oceanic and atmospheric anomalies in the northeast Pacific during the El Niño and La Niña events of 1995–2001, *Prog. Oceanogr.*, *54*, 459–491.

Simpson, J. J. (1983), Large-scale thermal anomalies in the California Current during the 1982–1983 El Niño, *Geophys. Res. Lett.*, *10*, 937–940, doi:10.1029/GL010i010p00937.

Song, H., A. J. Miller, B. D. Cornuelle, and E. Di Lorenzo (2011), Changes in upwelling and its water sources in the California Current System driven by different wind forcing, *Dyn. Atmos. Oceans*, *52*, 170–191.

Stohl, A. (1998), Computation, accuracy and applications of trajectories: A review and bibliography, *Atmos. Environ.*, *32*, 947–966.

Strub, P. T., and C. James (2002), The 1997–1998 oceanic El Nino signal along the southeast and northeast Pacific boundaries: An altimetric view. *Prog. Oceanogr.*, *54*, 439–458.

Uppala, S. M., et al. (2005), The ERA-40 re-analysis, *Q. J. R. Meteorol. Soc.*, *131*, 2961–3012.

Veneziani, M., C. A. Edwards, and A. M. Moore (2009), A central California coastal ocean modeling study: 2. Adjoint sensitivities to local and remote forcing mechanisms, *J. Geophys. Res.*, *114*, C04020, doi:10.1029/2008JC004775.

Verdon, D. C., and S. W. Franks (2006), Long-term behaviour of ENSO: Interactions with the PDO over the past 400 years inferred from paleoclimate records, *Geophys. Res. Lett.*, *33*, L06712, doi:10.1029/2005GL025052.